Nonideal parasitic resistance effects in bulk heterojunction organic solar cells

John R. Tumbleston,[1] Doo-Hyun Ko,[2] Edward T. Samulski,[2] and Rene Lopez[1,a)]
[1]*Department of Physics and Astronomy, University of North Carolina–Chapel Hill, Chapel Hill, North Carolina 27599, USA*
[2]*Department of Chemistry, University of North Carolina–Chapel Hill, Chapel Hill, North Carolina 27599, USA*

(Received 22 June 2010; accepted 29 August 2010; published online 28 October 2010)

A common assumption in both experimental measurements and device modeling of bulk heterojunction (BHJ) organic solar cells is that parasitic resistances are ideal. In other words, series resistance (R_{sr}) is near zero while shunt resistance (R_{sh}) approaches infinity. Relaxation of this assumption affects device performance differently depending on the chosen BHJ material system. Specifically, the impact of nonideal R_{sr} is controlled by the electric field dependence of the probability of charge transfer (CT) state dissociation (P_{CT}). This is demonstrated by evaluating the experimental current density versus voltage response within the framework of a drift/diffusion model for two BHJ systems that strongly differ in P_{CT}. Second, light intensity measurements of devices with nonideal R_{sr} and R_{sh} are shown to convolute the scaling of short-circuit current and open-circuit voltage with light intensity, which is a common technique to study BHJ device physics. Finally, we show the connection between the drift/diffusion and equivalent circuit model with regard to each model's treatment of CT state dissociation. In particular, the equivalent circuit model utilizes a light intensity dependent R_{sh} to describe this dissociation process and predicts a photocurrent under reverse bias that exceeds the photocurrent permitted by light absorption. © *2010 American Institute of Physics*. [doi:10.1063/1.3494100]

I. INTRODUCTION

The power conversion efficiency (PCE) of bulk heterojunction (BHJ) organic photovoltaics (OPV) has steadily improved from 4.4% in 2005 (Ref. 1) to values approaching 8.0% in 2010.[2] Developments in polymer design,[3] morphology control,[4] and device architecture[5] have paved the way toward benchmark efficiencies of 10%. Furthermore, rapid progress in characterizing both the photovoltage[6] and photogenerated current[7] in terms of fundamental physics has shed new light on device operation and provided new pathways to enhanced performance.

The underlying intricacy of device operation has lead to the use of multiple models to predict the current density versus voltage (J-V) behavior under different levels of illumination. For example, drift/diffusion formalisms have been proposed[8] and used extensively[9–11] to describe charge transfer (CT) state dissociation and free carrier transport. On the other hand, the equivalent circuit model[12] is commonly applied in part due to its relative ease of implementation.[4,13,14]

A primary difference between these two modes of description is their treatment of parasitic resistances. While the series (R_{sr}) and shunt (R_{sh}) resistances are clearly defined parameters in the equivalent circuit model, they are assumed to be ideal in drift/diffusion approaches. In other words, R_{sr} is near zero, while R_{sh} approaches infinity. Since drift/diffusion models capture more of the fundamental physics of BHJ solar cells, it is imperative to systematically explore the impact of relaxing these conditions. Given that different photoactive materials have different intrinsic properties, it is important to determine the influence of nonideal parasitic resistances for different BHJ solar cells.

Furthermore, it is not widely recognized that nonideal parasitic resistances could affect standard measurement techniques, such as the scaling of open-circuit voltage (V_{oc}) and short-circuit current (J_{sc}) to light intensity. These are commonly related to underlying physical mechanisms like bimolecular recombination of photogenerated carriers,[15,16] CT state dissociation,[17] and charge trapping effects,[18] so it is important to set the regimes where the assumption of ideality is valid.

Finally, even though there is widespread use of each type of model to explain OPV operation, there has been little work to determine relationships between the way each describes fundamental processes. For example, it is widely believed that CT state dissociation is a critical process in photocurrent output for BHJ solar cells, regardless of donor and acceptor material.[16] The signature of this process is a photocurrent that increases under reverse bias and eventually saturates.[19] In the equivalent circuit model, a nonideal R_{sh} fits this trend around short-circuit,[20,21] while an electric field dependent probability of CT state dissociation (P_{CT}) from Onsager–Braun theory[22] is utilized in the drift/diffusion approach.[8] Up to now, no relationship has been posited between these two descriptions.

In this work, we show that nonideal R_{sr} affects device performance differently depending on the actual electric field dependence of P_{CT}. This is demonstrated by evaluating the J-V response for two BHJ systems, poly(3-hexylthiophene) (P3HT) and poly(2-methoxy-5-(3′,7′-dimethyloctyloxy)-

a)Electronic mail: rln@physics.unc.edu.

p-phenylene vinylene) (MDMO-PPV) each combined with phenyl-C61-butyric acid methyl ester (PCBM). These two material combinations represent extremes in BHJ behavior, where P_{CT} for P3HT:PCBM has a weaker field dependence than that for MDMO-PPV:PCBM. Ultimately, this causes an increase in J_{sc} and heightened sensitivity to R_{sr}. Second, light intensity measurements of devices with nonideal R_{sr} and R_{sh} are shown to convolute the scaling of both J_{sc} and V_{oc}. In particular, the J_{sc} dependence becomes sublinear under high R_{sr}, while the V_{oc} deviates from the usual logarithmic behavior for low R_{sh}. Finally, we demonstrate the connection between the drift/diffusion and equivalent circuit model with regard to each model's treatment of CT state dissociation. In particular, the equivalent circuit model utilizes a light intensity dependent R_{sh} and thus predicts a photocurrent under reverse bias that exceeds that permitted by light absorption.

II. MODELING DEVICE RESISTANCES

Frequently, explanations for device J_{sc}, V_{oc}, and fill factor (FF) are linked to altered R_{sr} and R_{sh}. For example, inserting electron and/or hole transporting layers between the photoactive layer and electrodes can increase PCE where a reduction in R_{sr} is commonly cited.[23–25] Likewise, a low R_{sh} has been used to explain pinhole shorting through the photoactive layer.[1,21] These explanations are conveniently tied to the equivalent circuit model where R_{sr} and R_{sh} are included in a simple mathematical framework. Even though more complicated multiple diode[26] and mobility-dependent models[27] have been utilized, the most basic equivalent circuit model for BHJ solar cells[13] was developed for inorganic devices[12]

$$J = J_0\left[\exp\left(\frac{e(V_{app} - JR_{sr})}{nk_BT}\right) - 1\right] + \frac{V_{app} - JR_{sr}}{R_{sh}} - J_{photo}, \tag{1}$$

where J is the measured current density, J_0 is the reverse saturation current density, e is the elementary charge, n is the diode ideality factor, k_B is Boltzmann's constant, T is the temperature, V_{app} is the applied voltage, and J_{photo} is the voltage-independent photogenerated current density.

While this model simply incorporates device resistances, it does not elucidate the underlying physics of photocurrent generation, e.g., CT state dissociation and free carrier transport. Recently, these processes have been incorporated in an effective medium approach,[8] which includes a solution to Poisson's and the current continuity equations whereby electrons and holes move via drift and diffusion toward their respective electrodes. Before carrier collection, photogenerated carriers have some probability of dissociation in the internal electric field (P_{CT}) as dictated by Onsager–Braun theory[22] and must escape Langevin-type bimolecular recombination (B_{photo}) during transit.[28] The net photogeneration rate (U) for electrons and holes takes the form[8]

$$U = P_{CT}G - (1 - P_{CT})B_{photo}, \tag{2}$$

where G is the exciton generation rate dictated by light absorption. Although there has been widespread use of this model for BHJ systems, the accuracy of both P_{CT} (Refs. 29 and 30) and B_{photo} (Refs. 31 and 32) in an effective medium formalism are still under intense debate.[11,33]

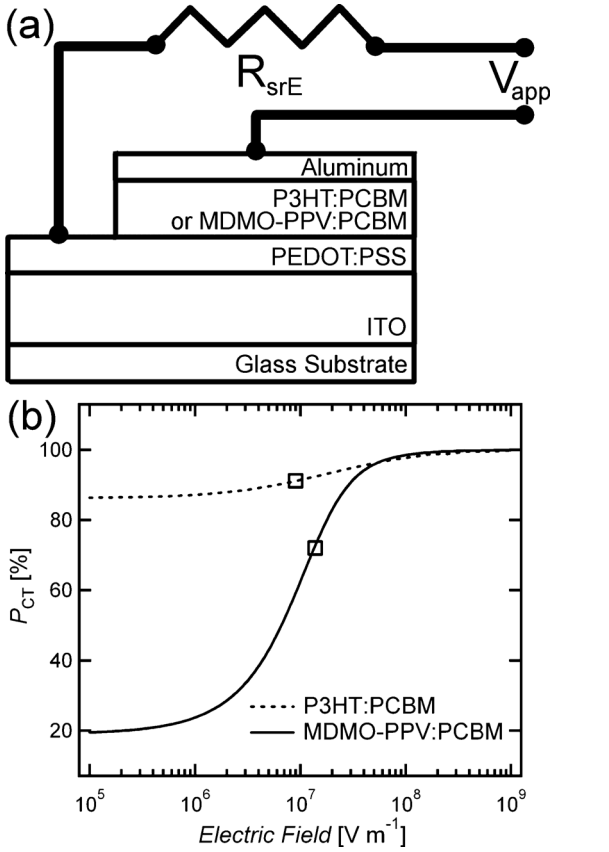

FIG. 1. (a) Schematic of experimental setup where a variable external resistor (R_{srE}) is connected in series with BHJ devices. (b) Dissociation probability of CT state (P_{CT}) for both P3HT:PCBM and MDMO-PPV:PCBM from Onsager–Braun theory. Squares represent P_{CT} under short-circuit conditions for $R_{sr} \to 0\ \Omega\ \text{cm}^2$.

In order to demonstrate the impact of nonideal resistances for different BHJ systems, we choose to focus on R_{sr}. As opposed to nonideal R_{sh}, R_{sr} has a greater influence on device performance under light intensities approaching 1 sun as will be discussed below. For this reason, R_{sr} is more commonly employed as an explanation for poor device performance. In the equivalent circuit model, an increase in R_{sr} essentially reduces the potential difference across the device. This reduction can be incorporated into the drift/diffusion framework by adding a term to the voltage boundary conditions applied at the anode and cathode ends of the photoactive layer

$$V_{\text{anode}} - V_{\text{cathode}} = V_{\text{gap}} - (V_{app} - JR_{sr}), \tag{3}$$

where V_{gap} is the built-in voltage set by the energy levels of the donor/acceptor system, V_{app} is the applied voltage, and J is the extracted current density dependent on V_{app}. This modification to the boundary conditions insures that V_{oc} will be independent of R_{sr} as is the case for the equivalent circuit model.[13] At open-circuit, $J=0$, so there is no modification to the boundary condition at this voltage.

In order to control R_{sr}, a variable external resistance load, R_{srE}, was connected in series with the BHJ devices and adjusted from 0 Ω to 1×10^4 Ω as shown in Fig. 1(a). Cur-

TABLE I. Parameters used for drift/diffusion (top section) and equivalent circuit (bottom section) modeling of devices with P3HT:PCBM and MDMO-PPV:PCBM as the photoactive layer.

Parameter	Symbol (unit)	P3HT:PCBM	MDMO-PPV:PCBM	Method
Electron mobility	$\mu_n(m^2\ V^{-1}\ s^{-1})$	2.0×10^{-7}	2.5×10^{-7}	[35,8]
Hole mobility	$\mu_p(m^2\ V^{-1}\ s^{-1})$	1.5×10^{-8}	3.0×10^{-8}	[35,8]
Exciton generation rate	$G(m^{-3}\ s^{-1})$	7.3×10^{27}	3.9×10^{27}	Measured
Built-in voltage	$V_{gap}(V)$	0.90	1.24	Fit
Active layer thickness	$t(m)$	1.0×10^{-7}	9.0×10^{-8}	Measured
e/h pair separation distance	$a(m)$	1.8×10^{-9}	3.2×10^{-9}	Fit
e/h pair decay rate	$k_f(s^{-1})$	2.0×10^{4}	1.3×10^{8}	Fit
Dielectric constant	$\epsilon(C^2\ N^{-1}\ m^{-2})$	3.0×10^{-11}	3.0×10^{-11}	[35,8]
Temperature	$T(K)$	300	300	Measured
Density of states	$N_0(m^3)$	2.5×10^{25}	2.5×10^{25}	[8]
Diode ideality factor	n(unitless)	n/a	2.0	[36]
Reverse saturation current	$J_0(A\ m^{-2})$	n/a	1.0×10^{-5}	Fit

rent measurements were then performed under variable applied bias and light intensity. The two BHJ active materials chosen herein, MDMO-PPV:PCBM and P3HT:PCBM, were selected based on their different field dependencies of P_{CT}.[15] In the Braun–Onsager approach, P_{CT} is dependent on the internal electric field as shown in Fig. 1(b). Two parameters that control the field dependence of P_{CT}, both the electron/hole pair separation distance (a) and decay rate (k_f) were fit to match the measured current under illumination (J_{light}). The field dependence of P_{CT} qualitatively matches that reported for P3HT:PCBM (weak field dependence) (Ref. 15) and MDMO-PPV:PCBM (strong field dependence).[8] All model parameters are listed in Table I including the method of determination [i.e., independently measured, fit to the illuminated current density (J_{light}), or taken from literature]. It should be noted that the exciton generation rate (G) and active layer thickness (t) were measured independently by applying an optical model to the measured device reflection[10,34] using optical properties determined from spectroscopic ellipsometry. Parameters in Table I are used for all model predictions in this work.[35,36] Finally, in the comparison between the equivalent circuit and drift/diffusion models, parameters for the equivalent circuit model were required for MDMO-PPV:PCBM devices and are given at the bottom of Table I.

III. EXPERIMENTAL

Devices were prepared by first sonicating indium tin oxide (ITO)-coated (140 nm) glass substrates in acetone, isopropyl alcohol, and distilled water for 10 min each and then dried in an oven overnight (150 °C). Next, the cleaned substrates were treated with UV ozone for 20 min (UVO Cleaner 42, Jelight Co. Inc.). A solution of poly(3,4-ethylenedioxythiopene):poly(styrenesulfonate) (PEDOT:PSS) (Baytron PH500) was then spin coated (40 nm) and annealed in air at 140 °C for 10 min. The samples where then moved to an inert gas (purified nitrogen) glove box where a solution of either P3HT (15 mg ml^{-1}) and PCBM (12 mg ml^{-1}) or MDMO-PPV (4 mg ml^{-1}) and PCBM (16 mg ml^{-1}) in chlorobenzene was spin coated on the ITO/PEDOT:PSS coated substrates. Finally, the devices were transferred to a vacuum chamber (2×10^{-6} torr) where 90 nm of Al was deposited on defined cell areas (12 mm^2). P3HT:PCBM devices were annealed at 150 °C for 30 min in the glove box prior to characterization.

IV. RESULTS AND DISCUSSION

A. Influence of nonideal R_{sr}

Figure 2 shows the modeled and experimental J-V characteristics under AM 1.5 illumination for devices with P3HT:PCBM and MDMO-PPV:PCBM as the photoactive layer with varying R_{sr}. Here, R_{sr} is determined by taking the inverse slope of the experimental data roughly 0.2 V higher in bias than open-circuit. These values are then used in Eq. (3) of the drift/diffusion model to simulate the J-V curves. While there is slight overestimation in taking the slope at these voltages compared to higher ones near 2 V (Ref. 1), it is more accurate than the common approach of taking the slope at open-circuit,[25] and protects against device breakdown during repeated measurements. From this figure, one can observe that the modification to the voltage boundary condition [Eq. (3)] is an appropriate way to model R_{sr} in the drift/diffusion formalism. Not only does V_{oc} remain constant, but changes in R_{sr} closely match those of the known external resistor, R_{srE}.

Figure 3 shows J_{sc}, FF, and PCE as functions of R_{sr} for both P3HT:PCBM and MDMO-PPV:PCBM devices. As R_{sr} increases, there are cross-over points for all three measures of performance where MDMO-PPV:PCBM devices outperform P3HT:PCBM solar cells. Furthermore, the J_{sc} is less affected than the FF under increasing R_{sr} for both device types. While this is a well known result for the equivalent circuit model,[13] it is not expected that there would be such striking differences between the two types of BHJ solar cells. In particular, the FF of MDMO-PPV:PCBM devices is less sensitive to R_{sr}: it exhibits a more gradual decline with increasing R_{sr}. Likewise, the FF for P3HT:PCBM devices begins to drop almost immediately compared to MDMO-PPV:PCBM solar cells and reaches the minimum of 25% at a much lower R_{sr} value.

These observations are attributed to the combination of differing field dependencies of P_{CT} [see Fig. 1(b)] and light

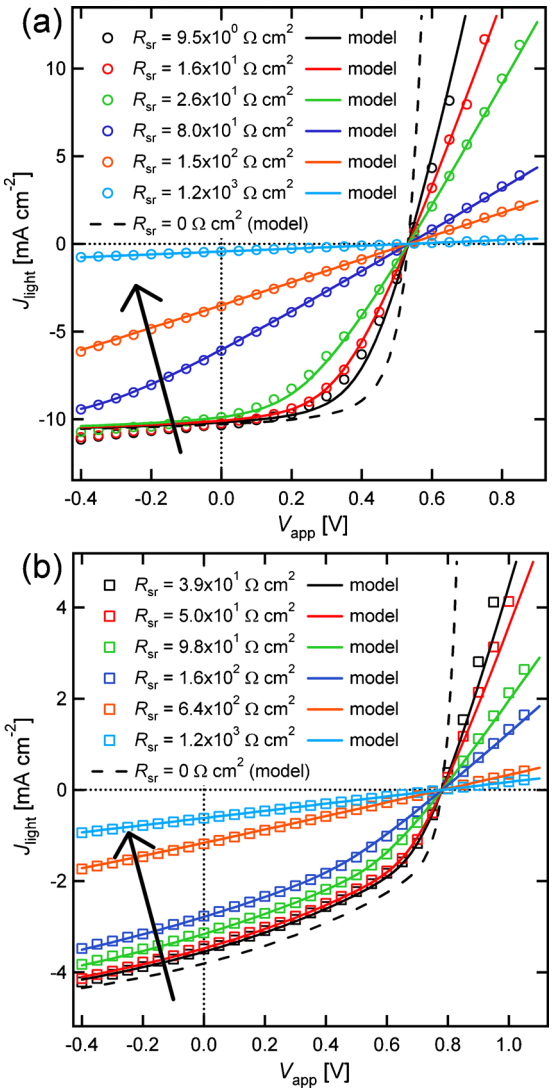

FIG. 2. (Color online) Experimental and modeled *J-V* curves for (a) P3HT:PCBM and (b) MDMO-PPV:PCBM as the photoactive layer with different R_{sr}. Arrows indicate increasing R_{sr}. Models are derived from the drift/diffusion approach using the electric field dependent probability of CT state dissociation (P_{CT}) of Fig. 1(b).

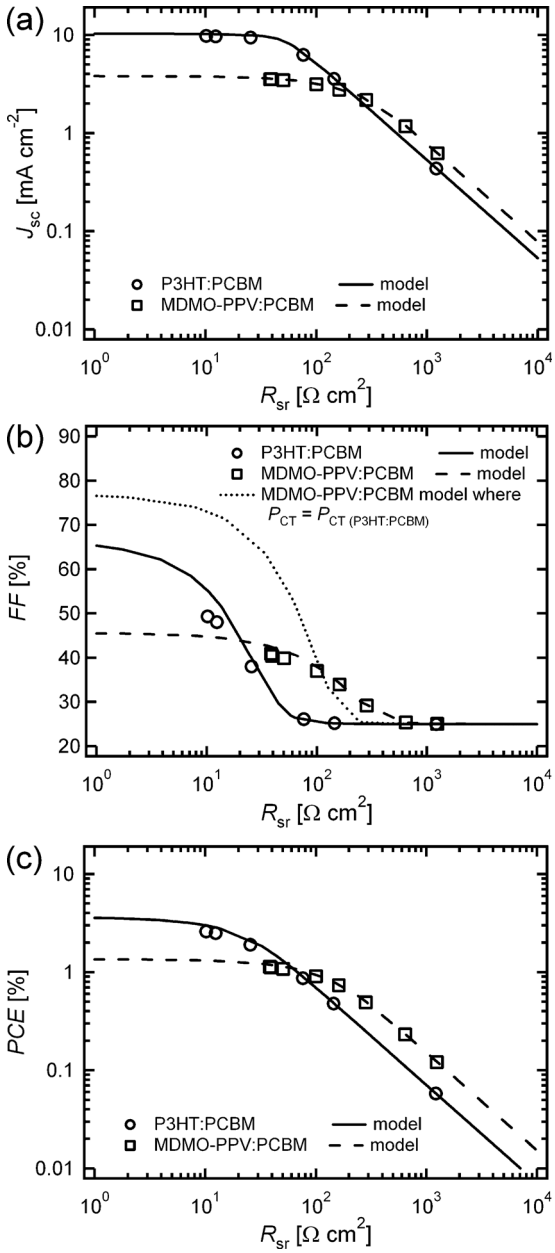

FIG. 3. (a) J_{sc}, (b) FF, and (c) PCE of devices with P3HT:PCBM and MDMO-PPV:PCBM as the photoactive layer under 1 sun conditions as functions of R_{sr}. A fictitious MDMO-PPV:PCBM device where P_{CT} is replaced with that of P3HT:PCBM is also given for FF in (b).

absorption. First, for ideal R_{sr}, a weak P_{CT} field dependence is desired, so that the photocurrent, which is proportional to P_{CT}, will remain high at maximum power point. This will result in a high FF. However, as R_{sr} increases away from ideality, a strong field dependence, as is the case for MDMO-PPV:PCBM, causes the photocurrent to drop at both short-circuit and maximum power point. This results in a FF that is less sensitive to R_{sr}. Further insight is gained by simulating a fictitious MDMO-PPV:PCBM solar cell where P_{CT} is replaced with that for P3HT:PCBM. Compared to actual MDMO-PPV:PCBM devices, the weaker P_{CT} field dependence causes the FF to increase from 45% to 77% for $R_{sr} \rightarrow 0$ Ω cm^2 [see Fig. 3(b)]. However, the FF also undergoes a sharper decline for increasing R_{sr}, which closely resembles the dependence for P3HT:PCBM devices. This signifies that a weak field dependence of P_{CT} is required to achieve high FF values under ideal R_{sr}, but for nonideal R_{sr}, a stronger field dependence can be advantageous to device performance. Furthermore, light absorption, as quantified by the $G \cdot t$ product (see Table I), can also limit the FF for ideal R_{sr} as evidenced by comparing P3HT:PCBM devices with the fictitious MDMO-PPV:PCBM solar cell model. The FF dependence effectively shifts up and to the right for lower light absorption when comparing these two devices [see Fig. 3(b)].

B. Nonideal resistances and light intensity measurements

In this section, the relationship between nonideal resistances and light absorption is more systematically explored by analyzing the light intensity dependence of the current output. Frequently, light intensity is related to J_{sc} through a

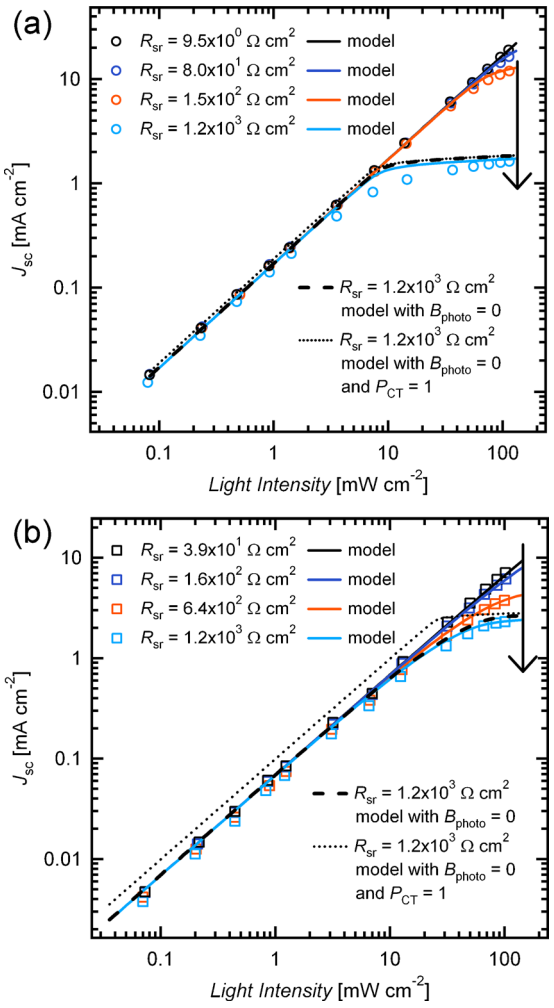

FIG. 4. (Color online) Light intensity dependence of J_{sc} for devices with (a) P3HT:PCBM and (b) MDMO-PPV:PCBM as the photoactive material where arrows indicate increasing R_{sr}. Model predictions are also given where $B_{photo}=0$ along with simulations of ideal devices where $P_{CT}=1$ for all electric fields and $B_{photo}=0$.

power law relationship.[16,37–39] Nonlinearities can indicate significant bimolecular recombination (B_{photo}) that can even induce space-charge limited behavior.[40]

Figure 4 shows the light intensity dependence and drift/diffusion model predictions of J_{sc} for both P3HT:PCBM and MDMO-PPV:PCBM devices under variable $\lambda=532$ nm laser illumination. The response is linear over the entire range for the lowest R_{sr} and becomes sublinear for high light intensity as R_{sr} increases. Usually, the sublinearities would be due to significant B_{photo} as is often the case when this type of behavior is observed. However, when the nonlinear regions are fit to a power law, the exponent is below that for a space-charge limited device (i.e., 0.75) (Ref. 40) and approaches logarithmic behavior, which is typically observed for V_{oc},[17] not J_{sc}.

The physical explanation for the nonlinearity can be probed by turning off bimolecular recombination in the model [i.e., setting B_{photo} in Eq. (2) to zero] for the most nonlinear case of $R_{sr}=1.2\times10^3$ Ω cm^2. If there is significant loss due to B_{photo}, then the current predicted from the model should increase in the nonlinear region and again become linear when B_{photo} is eliminated. However, near 100 mW cm^{-2} the model prediction only increases by about 10% for both P3HT:PCBM and MDMO-PPV:PCBM devices. Going a step further, P_{CT} may also be equated to unity for all electric fields, which, when combined with $B_{photo}=0$, eliminates all photocurrent loss processes in the simulation. Interestingly, the J_{sc} only increases slightly and still retains nonlinear behavior for this ideal case. Even though these measurements are carried out at short-circuit, when they are analyzed with regard to the effective applied voltage [i.e., $V_{app}-JR_{sr}$ in Eqs. (1) and (3)], it becomes clear that for high R_{sr}, the short-circuit measurement actually approaches open-circuit conditions. Thus, the dark or injected current begins to cancel the photogenerated current as R_{sr} increases even at short-circuit. This indicates that the light intensity scaling of J_{sc} for high R_{sr} should resemble that of V_{oc}, which explains the observed logarithmic behavior.

From these results, assuming that R_{sr} is ideal when scaling J_{sc} to light intensity is justified if R_{sr} is below 1.0×10^2 Ω cm^2. For R_{sr} above this value, it would not be possible to distinguish between B_{photo} and the cancellation of J_{sc} by the dark current, which both cause nonlinearities in the light intensity scaling. For some reported devices, interface and contact resistances reach this level.[4,14] Furthermore, the photocurrent near maximum power point is also frequently scaled to light intensity by assuming $J_{photo}=|J_{light}-J_{dark}|$.[15,16] However, this approximation becomes invalid for sufficiently large R_{sr}, especially near maximum power point where even smaller R_{sr} losses can interfere with light intensity scaling.

Like nonideal R_{sr} under high light intensity, nonideal shunt resistance (R_{sh}) under low light intensity can modify the scaling of V_{oc}. Usually, this dependence is logarithmic[17] even though trapping and other effects can cause modifications.[18] The effect of nonideal R_{sh} is demonstrated by placing a known resistor in parallel with the device instead of in series. Figure 5(a) shows the effect of the J-V curve for P3HT:PCBM solar cells for an incident intensity of 27 mW cm^{-2} under $\lambda=532$ nm laser illumination. Here, R_{sh} is calculated from the inverse slope of the dark J-V curve.[1] Even though changes are hardly noticeable until values fall below $R_{sh}=1.0\times10^4$ Ω cm^2, the light intensity dependence of V_{oc} changes from logarithmic to linear behavior. Likewise, the drift/diffusion model is determined to assume an ideal R_{sh} of at least 1.0×10^{10} Ω cm^2. This assumption makes little difference in the J-V curve under illumination, but does impact the light intensity scaling of V_{oc}.

In contrast to the light intensity dependence of J_{sc} that is modified for nonideal R_{sr} under high light intensity, the light intensity dependence of V_{oc} shows greater deviation for nonideal R_{sh} in the low intensity regime. Thus, it is important to consider this effect when linking the light intensity dependence of V_{oc} to fundamental physical processes, especially under low illumination levels.[16,38] It may be difficult to decouple the effect of R_{sh} and other more fundamental processes that can each cause V_{oc} to scale differently from the usual logarithmic behavior.

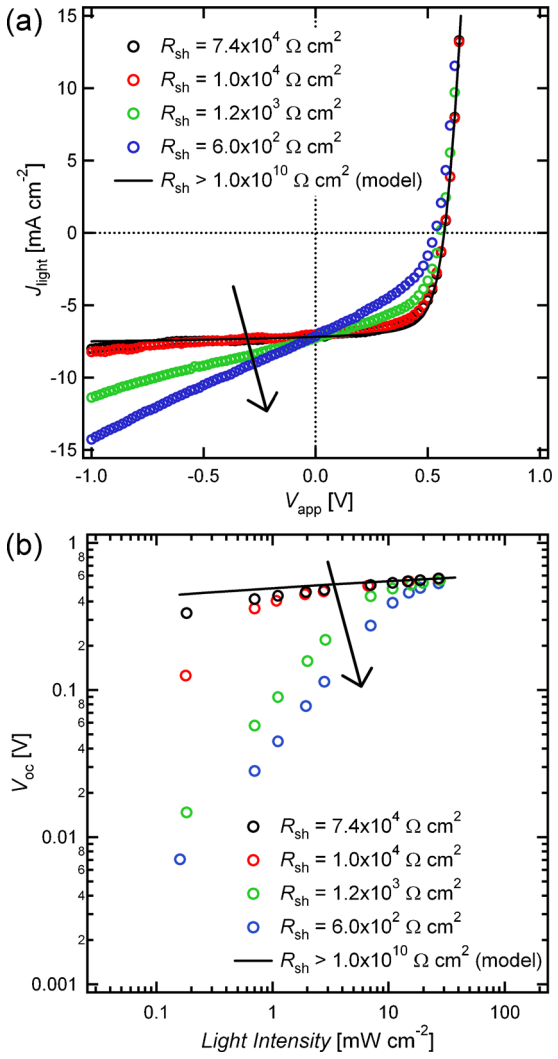

FIG. 5. (Color online) (a) *J-V* curve for P3HT:PCBM under 27 mW cm^{-2}, λ=532 nm laser illumination with varying levels of R_{sh} as determined from the inverse slope of the J_{dark} curves at short-circuit. Arrows indicate decreasing R_{sh}. (b) Light intensity dependence of V_{oc} where high R_{sh} results in the usual logarithmic behavior, while reduced R_{sh} causes the dependence to be linear for low light intensity.

C. Description of CT state dissociation in equivalent circuit and drift/diffusion models

Now that we have considered the light intensity scaling of both J_{sc} and V_{oc}, it is important to compare both the equivalent circuit and drift/diffusion model's treatment of CT state dissociation. The experimental signature of this process in the standard *J-V* measurement is a photocurrent that increases under reverse bias and eventually saturates. As previously explained in the drift/diffusion model, CT state dissociation is handled by the field dependence of P_{CT} as given by the Onsager–Braun formalism [Fig. 1(b)]. However, in the equivalent circuit approach, CT state dissociation can be modeled by splitting the shunt resistance under illumination, R_{shL}, into two parts, one that describes the shunt resistance in the dark, attributed to device pinholes and current leakage, R_{sh}, and another that handles CT state dissociation, R_{shCT}

$$R_{shL}^{-1} = R_{sh}^{-1} + R_{shCT}^{-1}. \quad (4)$$

Herein, we measure R_{shL} to be the inverse slope of the *J-V* curve at short-circuit under illumination. Likewise, R_{sh} is

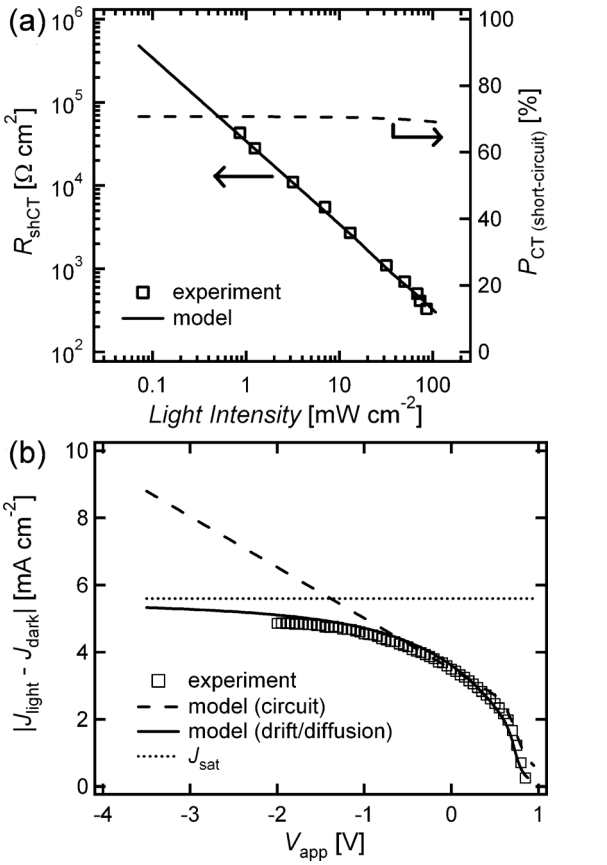

FIG. 6. (a) Experimental and modeled R_{shCT} that describes CT state dissociation in the equivalent circuit model [Eq. (1)] for devices with MDMO-PPV:PCBM as the active layer. In the drift/diffusion model, this corresponds to a P_{CT} that is independent of light intensity. (b) Experimental photocurrent ($|J_{light}-J_{dark}|$) of MDMO-PPV:PCBM devices with both equivalent circuit and drift/diffusion model predictions. At high reverse bias, the equivalent circuit prediction is larger than the saturated photocurrent (J_{sat}) that is dictated solely by light absorption.

taken as the inverse slope in the dark, which allows R_{shCT} to be calculated. As shown in the previous section, R_{sh} is determined to take values above 1.0×10^{10} Ω cm^2 in the drift/diffusion model. Furthermore, R_{shCT} has previously been related to device photoshunts[21] and was only recently used to describe CT state dissociation processes in the equivalent circuit approach.[20] For BHJ blends like MDMO-PPV:PCBM with strong P_{CT} field dependence, the slope at short-circuit is higher than for weakly dependent P_{CT} materials like P3HT:PCBM (see Fig. 2). In the equivalent circuit model, this leads to lower values of R_{shCT}.

Figure 6(a) gives the experimental light intensity dependence of R_{shCT} for MDMO-PPV:PCBM devices under various levels of λ=532 nm laser illumination. This result agrees with R_{shCT} calculations of the predicted *J-V* curves from the drift/diffusion model. However, under variation in light intensity, the drift/diffusion model does not require a light intensity dependent P_{CT}. On the contrary, a single field dependent function for P_{CT} is adequate. This is indicated in Fig. 6(a) by the constant P_{CT} determined at short-circuit. This comparison demonstrates the relationship between the drift/diffusion approach that uses a light intensity independent P_{CT} and the equivalent circuit model that incorporates light intensity dependent shunt resistance. For MDMO-

PPV:PCBM devices, $R_{shCT}=340\ \Omega\ cm^2$ under 100 mW cm^{-2} illumination corresponds to $P_{CT}=70\%$ at short-circuit.

While this straightforward relationship between each model's treatment of CT state dissociation bridges a gap between the two formalisms, the equivalent circuit model does make a prediction of the photocurrent that is unphysical. Here we assume $J_{photo}=|J_{light}-J_{dark}|$ as no external resistor was applied in series. As shown in Fig. 6(b), the experimental photocurrent for MDMO-PPV:PCBM under 1 sun conditions approaches a maximum value at high reverse bias, known as the saturated photocurrent (J_{sat}).[19] Here, the photocurrent is completely controlled by light absorption as high internal fields prohibit both monomolecular and bimolecular recombination losses. While the drift/diffusion model prediction also approaches J_{sat} under high reverse bias, the equivalent circuit model (parameters from Table I) predicts the photocurrent to exceed J_{sat}. This occurs due to the strong light intensity dependence of R_{shCT}, which causes R_{shL} to be much lower under illumination than in the dark. This result offers an argument against treatment of CT state dissociation as a modified shunt resistance in the equivalent circuit model.[20,21] For strongly field dependent P_{CT} materials like MDMO-PPV:PCBM, the low value of R_{shCT} needed to fit the *J-V* curve at short-circuit causes the photocurrent to exceed J_{sat}.

Even though reverse bias application is outside the range of power generation, this result is important when modeling other BHJ devices with strong field dependencies of P_{CT} and equivalently low R_{shCT}, such as low-band gap systems.[41] On the other hand, blends not limited by monomolecular recombination with a weak P_{CT} field dependence and high R_{shCT}, such as P3HT:PCBM (Ref. 13) and other high performing systems,[5,42] will cause the photocurrent to surpass J_{sat} only at reverse biases approaching device breakdown.

V. CONCLUSIONS

Herein, we have demonstrated the effects of relaxing the assumptions of ideal R_{sr} and R_{sh} in both device modeling and standard measurement techniques. Specifically, the drift/diffusion model assumes R_{sr} is near zero, where we demonstrate that increasing R_{sr} impacts device performance differently depending on the field dependence of P_{CT}. Second, light intensity measurements of devices with nonideal R_{sr} and R_{sh} obscure the scaling of J_{sc} and V_{oc} with light intensity, which is commonly tied to fundamental device physics. Finally, the equivalent circuit model utilizes a light intensity dependent R_{sh} to describe P_{CT} and thus predicts a photocurrent under reverse bias that exceeds the absorption-dictated saturated photocurrent. Further work might clarify other connections between these two models of BHJ solar cells.

ACKNOWLEDGMENTS

Support for this work is from NSF (Solar: Grant No. DMR-0934433) and UNC-Chapel Hill Institute for the Environment (Carolina Energy Fellows Program). Acknowledgment is also made to the donors of The American Chemical Society Petroleum Research Fund (Grant No. 49187-DNI10) for partial support of this research.

[1] G. Li, V. Shrotriya, J. Huang, Y. Yao, T. Moriarty, K. Emery, and Y. Yang, Nature Mater. **4**, 864 (2005).
[2] Y. Liang, Z. Xu, J. Xia, S.-T. Tsai, Y. Wu, G. Li, C. Ray, and L. Yu, Adv. Mater. (Weinheim, Ger.) **22**, E135 (2010).
[3] M. C. Scharber, D. Mühlbacher, M. Koppe, P. Denk, C. Waldauf, A. J. Heeger, and C. J. Brabec, Adv. Mater. (Weinheim, Ger.) **18**, 789 (2006).
[4] W. Ma, C. Yang, X. Gong, K. Lee, and A. J. Heeger, Adv. Funct. Mater. **15**, 1617 (2005).
[5] S. H. Park, A. Roy, S. Beaupre, S. Cho, N. Coates, J. S. Moon, D. Moses, M. Leclerc, K. Lee, and A. J. Heeger, Nat. Photonics **3**, 297 (2009).
[6] K. Vandewal, K. Tvingstedt, A. Gadisa, O. Inganäs, and J. V. Manca, Nature Mater. **8**, 904 (2009).
[7] T. M. Clarke and J. R. Durrant, Chem. Rev. (to be published).
[8] L. J. A. Koster, E. C. P. Smits, V. D. Mihailetchi, and P. W. M. Blom, Phys. Rev. B **72**, 085205 (2005).
[9] P. W. M. Blom, V. D. Mihailetchi, L. J. A. Koster, and D. E. Markov, Adv. Mater. (Weinheim, Ger.) **19**, 1551 (2007).
[10] D. W. Sievers, V. Shrotriya, and Y. Yang, J. Appl. Phys. **100**, 114509 (2006).
[11] R. Häusermann, E. Knapp, M. Moos, N. A. Reinke, T. Flatz, and B. Ruhstaller, J. Appl. Phys. **106**, 104507 (2009).
[12] J. Nelson, *The Physics of Solar Cells* (Imperial College Press, London, 2003).
[13] J. D. Servaites, S. Yeganeh, T. J. Marks, and M. A. Ratner, Adv. Funct. Mater. **20**, 97 (2010).
[14] T. Aernouts, W. Geens, J. Poortmans, P. Heremans, S. Borghs, and R. Mertens, Thin Solid Films **403–404**, 297 (2002).
[15] V. D. Mihailetchi, H. Xie, B. de Boer, L. J. A. Koster, and P. W. M. Blom, Adv. Funct. Mater. **16**, 699 (2006).
[16] R. A. Marsh, C. R. McNeill, A. Abrusci, A. R. Campbell, and R. H. Friend, Nano Lett. **8**, 1393 (2008).
[17] L. J. A. Koster, V. D. Mihailetchi, R. Ramaker, and P. W. M. Blom, Appl. Phys. Lett. **86**, 123509 (2005).
[18] M. M. Mandoc, W. Veurman, L. J. A. Koster, B. de Boer, and P. W. M. Blom, Adv. Funct. Mater. **17**, 2167 (2007).
[19] V. D. Mihailetchi, L. J. A. Koster, J. C. Hummelen, and P. W. M. Blom, Phys. Rev. Lett. **93**, 216601 (2004).
[20] J. D. Servaites, M. A. Ratner, and T. J. Marks, Appl. Phys. Lett. **95**, 163302 (2009).
[21] C. Waldauf, M. C. Scharber, P. Schilinsky, J. A. Hauch, and C. J. Brabec, J. Appl. Phys. **99**, 104503 (2006).
[22] C. L. Braun, J. Chem. Phys. **80**, 4157 (1984).
[23] S. Chaudhary, H. Lu, A. M. Muller, C. J. Bardeen, and M. Ozkan, Nano Lett. **7**, 1973 (2007).
[24] M. D. Irwin, D. B. Buchholz, A. W. Hains, R. P. H. Chang, and T. J. Marks, Proc. Natl. Acad. Sci. U.S.A. **105**, 2783 (2008).
[25] C. Tao, S. Ruan, G. Xie, X. Kong, L. Shen, F. Meng, C. Liu, X. Zhang, W. Dong, and W. Chen, Appl. Phys. Lett. **94**, 043311 (2009).
[26] S. Yoo, B. Domercq, and B. Kippelen, J. Appl. Phys. **97**, 103706 (2005).
[27] P. Schilinsky, C. Waldauf, J. Hauch, and C. J. Brabec, J. Appl. Phys. **95**, 2816 (2004).
[28] L. J. A. Koster, V. D. Mihailetchi, and P. W. M. Blom, Appl. Phys. Lett. **88**, 052104 (2006).
[29] D. Veldman, O. Ipek, S. C. J. Meskers, J. Sweelssen, M. M. Koetse, S. C. Veenstra, J. M. Kroon, S. S. van Bavel, J. Loos, and R. A. J. Janssen, J. Am. Chem. Soc. **130**, 7721 (2008).
[30] C. Deibel, T. Strobel, and V. Dyakonov, Phys. Rev. Lett. **103**, 036402 (2009).
[31] C. Groves and N. C. Greenham, Phys. Rev. B **78**, 155205 (2008).
[32] A. Pivrikas, G. Juska, A. J. Mozer, M. Scharber, K. Arlauskas, N. S. Sariciftci, H. Stubb, and R. Osterbacka, Phys. Rev. Lett. **94**, 176806 (2005).
[33] T. Kirchartz, B. E. Pieters, K. Taretto, and U. Rau, Phys. Rev. B **80**, 035334 (2009).
[34] G. Dennler, K. Forberich, M. C. Scharber, C. J. Brabec, I. Tomiš, K. Hingerl, and T. Fromherz, J. Appl. Phys. **102**, 054516 (2007).
[35] L. J. A. Koster, V. D. Mihailetchi, and P. W. M. Blom, Appl. Phys. Lett. **88**, 093511 (2006).
[36] C. G. Shuttle, A. Maurano, R. Hamilton, B. O'Regan, J. C. de Mello, and J. R. Durrant, Appl. Phys. Lett. **93**, 183501 (2008).
[37] A. Moulé and K. Meerholz, Appl. Phys. B: Lasers Opt. **92**, 209 (2008).
[38] C. R. McNeill, J. J. M. Halls, R. Wilson, G. L. Whiting, S. Berkebile, M. G. Ramsey, R. H. Friend, and N. C. Greenham, Adv. Funct. Mater. **18**, 2309 (2008).

[39]C. G. Shuttle, B. O'Regan, A. M. Ballantyne, J. Nelson, D. D. C. Bradley, and J. R. Durrant, Phys. Rev. B **78**, 113201 (2008).
[40]V. D. Mihailetchi, J. Wildeman, and P. W. M. Blom, Phys. Rev. Lett. **94**, 126602 (2005).
[41]M. Lenes, M. Morana, C. J. Brabec, and P. W. M. Blom, Adv. Funct. Mater. **19**, 1 (2009).
[42]H.-Y. Chen, J. Hou, S. Zhang, Y. Liang, G. Yang, Y. Yang, L. Yu, Y. Wu, and G. Li, Nat. Photonics **3**, 649 (2009).